american physiological society

JNP JOURNAL OF NEUROPHYSIOLOGY

J Neurophysiol 131: 1–15, 2024.
First published October 11, 2023; doi:10.1152/jn.00082.2023

RESEARCH ARTICLE

Control of Movement

Dynamic primitives in constrained action: systematic changes in the zero-force trajectory

James Hermus,[1] Joseph Doeringer,[2] Dagmar Sternad,[3] and Neville Hogan[1,4]

[1]*Department of Mechanical Engineering, Massachusetts Institute of Technology, Cambridge, Massachusetts, United States;* [2]*Vicarious Surgical, Waltham, Massachusetts, United States;* [3]*Departments of Biology, Electrical and Computer Engineering, and Physics, Northeastern University, Boston, Massachusetts, United States; and* [4]*Department of Brain and Cognitive Sciences, Massachusetts Institute of Technology, Cambridge, Massachusetts, United States*

Abstract

Humans substantially outperform robotic systems in tasks that require physical interaction, despite seemingly inferior muscle bandwidth and slow neural information transmission. The control strategies that enable this performance remain poorly understood. To bridge that gap, this study examined kinematically constrained motion as an intermediate step between the widely studied unconstrained motions and sparsely studied physical interactions. Subjects turned a horizontal planar crank in two directions (clockwise and counterclockwise) at three constant target speeds (fast, medium, and very slow) as instructed via visual display. With the hand constrained to move in a circle, nonzero forces against the constraint were measured. This experiment exposed two observations that could not result from mechanics alone but may be attributed to neural control composed of dynamic primitives. A plausible mathematical model of interactive dynamics (mechanical impedance) was assumed and used to "subtract" peripheral neuromechanics. This method revealed a summary of the underlying neural control in terms of motion, a zero-force trajectory. The estimated zero-force trajectories were approximately elliptical and their orientation differed significantly with turning direction; that is consistent with control using oscillations to generate an elliptical zero-force trajectory. However, for periods longer than 2–5 s, motion can no longer be perceived or executed as periodic. Instead, it decomposes into a sequence of submovements, manifesting as increased variability. These quantifiable performance limitations support the hypothesis that humans simplify this constrained-motion task by exploiting at least three primitive dynamic actions: oscillations, submovements, and mechanical impedance.

NEW & NOTEWORTHY Control using primitive dynamic actions may explain why human performance is superior to robots despite seemingly inferior "wetware"; however, this also implies limitations. For a crank-turning task, this work quantified two such informative limitations. Force was exerted even though it produced no mechanical work, the underlying zero-force trajectory was roughly elliptical, and its orientation differed with turning direction, evidence of oscillatory control. At slow speeds, speed variability increased substantially, indicating intermittent control via submovements.

constrained motion; dynamic primitives; mechanical impedance; oscillations; submovements

INTRODUCTION

Humans excel at physical interaction with objects, even when those objects introduce complex dynamics and kinematic constraints. Indeed, human dexterity exceeds that of most modern robots, despite the fact that information transmission in the human neuromechanical system is extremely slow, especially when compared with its robotic counterparts (1–3). Moreover, the human neuromotor system is noisy (4, 5). To date, motor neuroscience has primarily focused on unconstrained elementary behaviors, such as reaching in a horizontal plane, to ensure strict experimental control. Comparatively few studies have investigated physical interaction with objects in the environment that generate additional interactive dynamics (6–9). A kinematic constraint provides an intermediate stage between

Correspondence: J. Hermus (jhermus@mit.edu).
Submitted 22 February 2023 / Revised 2 October 2023 / Accepted 5 October 2023

0022-3077/24 Copyright © 2024 the American Physiological Society.

Downloaded from journals.physiology.org/journal/jn at EPFL Bibliotheque USD (128.179.253.225) on January 16, 2024.

unconstrained (free) motion and interaction with complex dynamics. Such constrained behaviors are ubiquitous in everyday manipulation as exemplified by the action of turning a steering wheel or opening a door. In fact, opening a door was reported to be the most common activity of daily living (10). This paper presents a study of unimpaired subjects physically interacting with a circular constraint, i.e., turning a crank.

A central challenge of behavioral motor neuroscience is to "dis-entangle" the contributions of neural control and biomechanics. Over the past decades, several robust features of human movement have been identified. Notable examples include Fitts' law or the speed-accuracy trade-off (11–14) and the speed-curvature relation or the two-thirds power law (15–19). These studies investigated conditions with free reaching (substantial motion, negligible force) or force exertion during static postures (substantial force, negligible motion). However, in everyday life, physical interaction frequently involves both substantial motion and substantial force. Is the control strategy adopted in physical interaction different from free movement (20)? In recent work on kinematically constrained movement, we demonstrated that when contributions from peripheral neuromechanics were subtracted, patterns seen in free motion reemerged during physical interaction (21).

Mechanical Impedance Provides Insight to Interactive Tasks

When a behavior involves substantial contact, force and motion are no longer independent variables (22). Force exerted on an object depends not only on neural activity but also on the object's motion. One way to describe the dynamics of interaction is with the mechanical impedance operator $Z\{\cdot\}$ (23). Mathematically, impedance[1] is the relation between displacement and the force it evokes, a dynamic generalization of stiffness. The force time-function $F(t)$ can be computed from the displacement time-function $\Delta x(t)$, $F(t) = Z\{\Delta x(t)\}$. Displacement is defined as $\Delta x(t) = x_0(t) - x(t)$, where $x(t)$ is the hand position, and $x_0(t)$ is a "zero-force trajectory." In principle, knowledge of mechanical impedance, in combination with simultaneous measurement of force and motion during object manipulation, would allow us to "subtract off" or "peel back" peripheral biomechanics. This uncovers a summary of one aspect of the underlying neural influences in terms of motion,

$$x_0 = Z^{-1}\{f\} + x \qquad (1)$$

In practice, mechanical impedance is nonlinear and time-varying. Measuring it during action can be achieved, but is challenging (25–30). Moreover, measurement introduces perturbations that may induce altered behavior. An alternative avenue, pursued here, is to approximate mechanical impedance using a plausible mathematical model based on measurements made under steady postural conditions. The model parameters are then varied over a substantial range to assess the sensitivity of the results to variations in mechanical impedance. Given this model and observations of actual motion and exerted force, we calculated the "zero-force trajectory." This is the trajectory that would have been followed if the external forces had been absent (zero). It summarizes one consequence of neural activity and expresses it as a quantity that may be compared with actual motion.

Previously, we applied this method to the task of turning a planar crank. A model of limb impedance was assumed and the zero-force trajectory was computed (21). The zero-force trajectory showed evidence of the speed-curvature relation reported in unconstrained motion, suggesting that our approach reveals information about neural control. However, structure beyond that of the speed-curvature relation was also evident in those data. The study reported here further investigated the zero-force trajectory during crank turning, emphasizing how it varied with turning direction and movement speed from fast to very slow.

The Paradox of Human Performance—Dynamic Primitives

Human reaction time to a visually perceived stimulus takes 150–200 ms or more depending on the action. Given the magnitude of these delays, the speed, agility, and precision observed in everyday activities is astonishing. Even an activity as simple as opening a door with one hand and maintaining a stable upright posture, and in some cases, holding a cup of coffee in the other hand, would seem impossible using conventional closed-loop feedback control. This is the paradox of human performance. The long delays indicate that humans rely heavily on a predictive or feedforward control strategy based on some internal representation or model of the system to be controlled (31, 32). However, it seems unlikely that humans develop a detailed "engineering-style" dynamic model for each object they interact with.

Mounting evidence indicates that human control is modular, composed of primitive actions (22, 33–40). Modules have been defined in different ways and at different levels of organization. One common definition proposes patterns of proportional activation of different muscle groups, i.e., synergies (41, 42). Another definition identifies subspaces of the skeletal configuration; confining motions to these subspaces achieves a simplifying reduction of dimensionality (43). Primitives have also been defined at a functional level as an action to be performed on a specific object such as grasping or pushing (39, 44–46).

It has been proposed that to achieve highly dynamic and dexterous performance despite neuromechanical limitations, human behavior is composed of dynamic primitives (37, 47–51). These are conceived as dynamic attractors (for example, limit-cycle oscillations) that emerge from nonlinear interactions between neural and mechanical parts of the system and, once evoked, require minimal intervention from higher levels of the central nervous system (CNS) (37, 52). In this theory, dynamic primitives are "building blocks" of complex actions. The parameters of these building blocks are encoded, facilitating human learning, performance, and retention of

[1]For brevity, the term "impedance" will always refer to "mechanical impedance." The term "preflex," introduced by Loeb et al. (24) similarly describes interactive mechanics but is confined to passive muscle properties, a component of mechanical impedance.

Downloaded from journals.physiology.org/journal/jn at EPFL Bibliotheque USD (128.179.253.225) on January 16, 2024.

complex skills. The primitives are simultaneously and sequentially combined to produce force and motion. In practice, this may be described by defining a zero-force trajectory composed of submovements and/or oscillations interacting with impedances in a Norton equivalent network (53).

Motivation for the Experiment

If dynamic primitives underlie physical interactions, quantifiable limitations may be evident in human performance, from which dynamic primitives may be inferred. Negotiating a circular constraint in a horizontal plane at constant speed requires periodic motion in each degree of freedom, either in joint space or hand space. We, therefore, anticipated that crank turning might preferentially be executed as a combination of oscillatory actions (not necessarily a superposition of Fourier components). Noncollinear sinusoids of the same period, but different amplitude and phase describe ellipses, a subset of the so-called Lissajous plots. Constant-speed circular hand motion requires sinusoidal motions in orthogonal directions with a phase offset of ±90° depending on the direction of motion. Our previous study of circular crank turning revealed zero-force trajectories with a roughly elliptical shape (35). As the motions evoked by neural oscillations would lag those neural oscillations to an extent determined by the dynamic behavior of the neuromechanical periphery, we expected different ellipses for motions in opposite directions. This study examined turning in both clockwise (CW) and counterclockwise (CCW) directions to test *hypothesis 1*: the zero-force trajectory describes a roughly elliptical path that has different orientations for CW and CCW rotations.

Despite the repeatability of the actions required to turn a crank, imperfect execution may be anticipated due to sensorimotor noise and/or inadequate prediction of inertial dynamics and neuromuscular response. The consequences of imperfect prediction of inertial dynamics and neuromuscular response should decline (precipitously) with decreasing speed: all inertial forces decline with the square of speed; velocity-dependent muscle dynamics decline in proportion to speed; therefore, slower speed allows ample time for feedback corrections. However, rhythmic actions with periods longer than 2 to 5 s are neither perceived nor executed as periodic (55, 56). Previous research has shown that slower movements, even if periodic, "break down" into a sequence of stereotyped submovements, possibly overlapping (33), another class of dynamic primitives. Consequently, despite the dynamic advantages of moving slowly, we anticipated that performance would be compromised during movements with a period substantially longer than 2–5 s. This motivated *hypothesis 2*: variability of hand speed will increase in the slowest movements.

METHODS

Participants

Ten healthy male college-age students were recruited for the study. All participants were right-handed, and none reported any biomechanical injury to their arm or any neurological problems. Before participating in the study, they were informed about the experimental procedure and signed an informed consent document. The protocol was approved by MIT's Institutional Review Board.

Experimental Apparatus

The experiment was the same as that described in Ref. 21. Subjects were seated and rotated a crank in a horizontal plane. Subjects sat in a chair with a rigid back, while the shoulder was constrained by a harness attached to the back of the chair (Fig. 1). Subjects were positioned such that the crank, with a radius of 10.29 cm, was well within the workspace of the arm. The upper arm was suspended by a canvas sling connected to the ceiling; both upper and lower arms were in the plane of the crank. During the experiment, the subject's arm was occluded from view by a wooden structure which did not limit the range of motion. Speed feedback was provided on a monitor mounted ~75 cm in front of the subjects' eyes.

The crank is shown in the inset of Fig. 1. The crank arm was mounted on a high-precision incremental optical encoder/interpolator set (Gurley Precision Instruments encoder #8335–11250-CBQA, interpolator #HR2-80QA-BRD) with a resolution of 0.0004° per count. A six-axis force transducer (ATI Model 15/50) was attached to the end of the crank, with a handle mounted on it. A spool managed the force transducer cable.

Data acquisition was controlled by a computer running the QNX real-time operating system on an Intel Pentium 100 processor. The encoder, sampling at 200 Hz, was connected to a set of counters and to the computer via digital I/O. The ATI force transducer's signal, sampled at 100 Hz, was processed by its embedded controller and input to the computer through the digital I/O. This visual display was also generated by the computer and was presented on a 17-in. monitor (311 × 238 mm, resolution 1,280 × 1,024, 76 Hz).

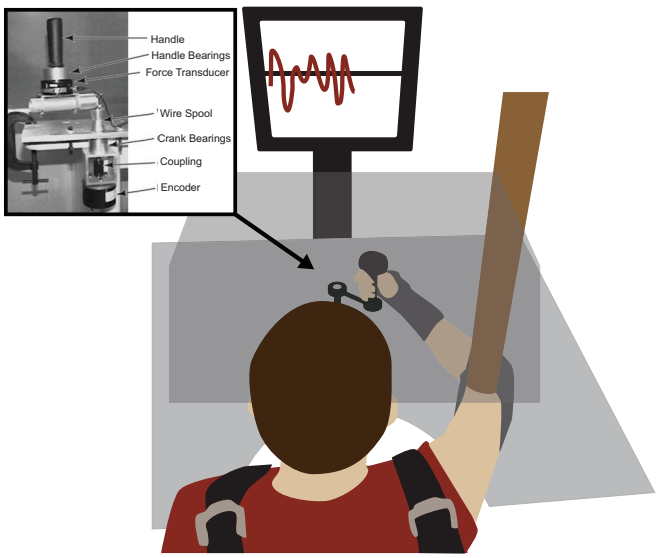

Figure 1. Experimental setup showing how the subject was seated in front of the crank. Vision of the arm and crank was occluded. The subject was provided with real-time speed feedback on a monitor in front of them. The wrist was braced to eliminate wrist movements, the elbow was supported by a sling to ensure the horizontal configuration of the arm aligned with the crank, and the shoulders were strapped to a chair. The crank provided a circular constraint.

Downloaded from journals.physiology.org/journal/jn at EPFL Bibliotheque USD (128.179.253.225) on January 16, 2024.

Experimental Design and Procedure

Subjects were instructed to move their hand around the circular crank with constant speed. Visual feedback on the monitor displayed the target speed, as well as subjects' real-time hand speed. The horizontal axis was time, and the vertical axis was speed. Target speed was displayed as a horizontal line in the middle of the screen. Subjects' speed was estimated using a backward finite-difference algorithm. The relation between crank motion and screen display was rescaled for every block; the width of the screen corresponded to the time of the trial, which was a function of the desired crank speed.

At the start of the experiment, subjects familiarized themselves by performing 20 trials at their preferred speed, 10 trials in clockwise direction (CW) and 10 in counterclockwise direction (CCW); each trial lasted 8 s. Subjects were not provided any visual feedback during this first set of trials. For the experiment proper, subjects performed six blocks of 30 trials, each with visual specification of one of three target speeds (slow: 0.075, medium: 0.5, and fast: 2.0 revolutions per second), in either CW or CCW directions. The order of the speed and direction blocks was randomized across subjects. The three speeds were selected to cover a wide range: 0.075 rev/s was extremely slow (required over 13 s per revolution), 0.5 rev/s was close to subjects' preferred speed, and 2.0 rev/s was close to the fastest subjects could turn the crank.

In the slow-speed conditions, each trial lasted 45 s; in the medium-speed conditions, each trial lasted 16 s; in the fast-speed conditions, each trial lasted 4 s. This yielded eight turns of the crank for the fast and medium conditions, but only ~3.4 turns of the crank for the slow condition. The duration of the slow-speed trials was chosen as a compromise between acquiring adequate data and avoiding subject fatigue. Seven trials in each block were "blind" catch trials, randomly interspersed, in which visual feedback of the actual hand speed was removed, while the display of the target speed was retained.

Extraction of Zero-Force Trajectories

To obtain the zero-force trajectories, a simplified model of muscle mechanical impedance was used, a linear spring and viscous damping element with common displacement (57). To implement this model on a two-joint arm, joint stiffness was assumed to be a 2×2 symmetric matrix, independent of configuration. Joint damping, also a 2×2 symmetric matrix, was proportional to joint stiffness. The assumption of a constant joint space stiffness provided a sufficient approximation of the variation of hand stiffness with position (58). These assumptions are similar to the muscle model previously used by Flash (59), but in this case, we used a damping term which was defined relative to the joint space zero-force trajectory $\boldsymbol{q}_0$.[2]

The joint torque was defined by

$$\tau = \boldsymbol{K}(\boldsymbol{q}_0 - \boldsymbol{q}) + \boldsymbol{B}(\dot{\boldsymbol{q}}_0 - \dot{\boldsymbol{q}}) \quad (2)$$

The stiffness in units of N-m/rad was defined as

$$\boldsymbol{K} = G\begin{bmatrix} K_{11} & K_{12} \\ K_{21} & K_{22} \end{bmatrix} = G\begin{bmatrix} 29.5 & 14.3 \\ 14.3 & 39.3 \end{bmatrix} \quad (3)$$

The viscous damping in units of N-m-s/rad was defined as

$$\boldsymbol{B} = \begin{bmatrix} B_{11} & B_{12} \\ B_{21} & B_{22} \end{bmatrix}. \quad (4)$$

K_{11} and B_{11} were the net shoulder joint stiffness and damping, K_{12}, B_{12}, K_{21}, and B_{21} were the two-joint parameters, and K_{22} and B_{22} described the elbow parameters; G was a dimensionless scalar. The values for joint stiffness and damping were consistent with those of Flash (59), such that $\boldsymbol{B} = \beta\boldsymbol{K}$. The β term had units of time, consistent with a first-order model of muscle impedance (60). A gain of $G = 0.5$ was used in the slow and medium cases, and a gain of $G = 1.5$ was used in the fast case. Note that the effect of the values of G on the zero-force trajectories was further tested (see below). Damping was derived from stiffness by multiplication by a constant factor β, which was 0.05 s for the slow and medium cases, and 0.1 s for the fast cases.

Dynamic equations describing the inertial mechanics of a planar two-segment model of the upper limb constrained by a crank are presented in APPENDIX B. The Cartesian hand position was denoted by $\boldsymbol{x} = [x, y]^T$, the joint position was denoted by $\boldsymbol{q} = [q_1, q_2]^T$, the crank position was denoted as θ, and the radius of the crank was denoted as r. The crank normal unit vector $\boldsymbol{n}$ and tangential unit vector $\boldsymbol{e}$ are graphically defined in Figure A3. Substituting *Eq. 2* into *Eqs. 9*, *10*, and *11* (from APPENDIX B) yielded an expression for $\dot{\boldsymbol{q}}_0$:

$$\dot{\boldsymbol{q}}_0 = \boldsymbol{B}^{-1}\Big[\boldsymbol{M}\boldsymbol{J}^{-1}\Big[\{\boldsymbol{J}\boldsymbol{M}^{-1}\boldsymbol{J}^T + r^2 I^{-1}\boldsymbol{e}\boldsymbol{e}^T\}\boldsymbol{F} - \dot{\boldsymbol{J}}\dot{\boldsymbol{q}} - r\dot{\theta}(\dot{\theta}\boldsymbol{n} + b_c I^{-1}\boldsymbol{e})\Big] + \boldsymbol{h} - \boldsymbol{K}(\boldsymbol{q}_0 - \boldsymbol{q})\Big] + \dot{\boldsymbol{q}} \quad (5)$$

Further explanation of this equation can be found in APPENDIX B. Integrating *Eq. 5* enabled computation of the zero-force trajectory corresponding to a prescribed position, velocity, acceleration, and force.

The velocity and force signals were filtered with a second-order zero-phase-lag Butterworth filter using a cutoff frequency of 10 Hz, except in the slow condition. The tangential force in the slow condition was small in magnitude. At slow speeds, a large number of samples with a magnitude close to the resolution of the sensor were observed. This resulted in artifactual step changes in the force measurements. To eliminate these artifacts, the tangential force in the slow condition was filtered with a cutoff frequency of 0.5 Hz, far faster than the turning frequency of the slow task (0.075 rev/s).

Sensitivity to Impedance Assumptions

To the best of our knowledge, two-joint limb impedance measurements during physical interaction with a constraint have not been reported. Thus, impedance parameters were based on unconstrained static arm stiffness and single-joint damping measurements (61, 62). Consequently, the impedance parameters, the gain term for the stiffness, G, and the proportional damping term, β, were varied to test whether the results were sensitive to the impedance values used to compute the zero-force trajectory. When G and β changed, the zero-force trajectory was expected to change. However,

[2]The forward kinematics of this two-link model is a unique map from joint space to hand space such that, if the joint space zero-force trajectory q_0 is known, the hand space zero-force trajectory x_0 is also known.

Downloaded from journals.physiology.org/journal/jn at EPFL Bibliotheque USD (128.179.253.225) on January 16, 2024.

the main question was whether the dependent measures were robust to changes in the stiffness and damping. To this end, the dependent measure $\ln(r)_{PC}$ described below was computed when the G and β terms were each varied over a 3:1 range.

Dependent Measures

Orientation of zero-force trajectory.

In our prior work, the zero-force trajectory could be approximated by an ellipse. To quantify the orientation of an ellipse, the choice of coordinates required care. Two potential candidates are shown in Fig. 2. One choice of coordinates is the orientation of the major axis, θ_a, and the ellipse eccentricity, ϵ, the ratio of major and minor axis lengths. However, the major axis orientation is not defined uniquely for an eccentricity of unity and, for eccentricities near unity, the major axis angle is expected to have a nearly flat distribution spread over a wide range of angles. Furthermore, the distribution of the major axis angle and eccentricity are expected to be statistically dependent.

To address this concern, we used log-ratio coordinates, shown on the right in Fig. 2. Though less intuitive (further explanation is in APPENDIX A), they have numerical properties better suited to statistical analysis (63, 64). The ratio of lengths in any two fixed directions is expected to have an approximately log-normal statistical distribution. Thus, the logarithm of the ratio of lengths in any two fixed directions is expected to be approximately normally distributed. Furthermore, these distributions are expected to be statistically independent. The ln(ratio) coordinates determined at a 0° and 45° angle are denoted by $\ln(r_0)$ and $\ln(r_{45})$.

For each subject in each speed and direction condition, the zero-force trajectory was binned into 200 angular position bins. The average radial position was computed for each bin. This polar representation was used to estimate the lengths l_x, l_y, l_x', l_y' at 0° and 45°, respectively. The ratio between l_x/l_y was denoted as r_0 and the ratio between l_x'/l_y' was denoted as r_{45}, as illustrated in Fig. 2. For each subject and each condition, $\ln(r_0)$ and $\ln(r_{45})$ were estimated.

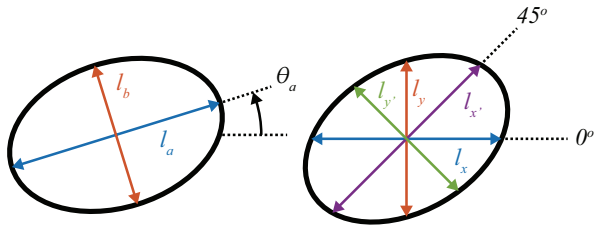

Figure 2. Two possible sets of coordinates: ellipse major axis orientation θ_a and eccentricity ϵ (*left*); log-ratio coordinates (*right*). θ_a is poorly defined when ϵ approaches unity. The log-ratio coordinates alleviate this problem. The length measures, which compose the log-ratio coordinates are l_x, l_y, l_x', l_y'. The subscripts x and y denote two orthogonal directions. The prime denotes the orientation of the x axis such that the first was as 0° and the second was at 45°. Then, r_0 was defined as l_x/l_y and r_{45} was defined as l_x'/l_y'.

However, the two dependent measures $\ln(r_0)$ and $\ln(r_{45})$ in the illustration were based on arbitrary choices of the reference angle. Therefore, principal component analysis (PCA) was performed to identify the coordinate that explained the most variance (see Fig. 6). This was justified because each log-ratio coordinate was expected to be statistically independent. To test *hypothesis 1*, $\ln(r)_{PC}$ served as the dependent measure for statistical analysis. A significant difference in this single coordinate was sufficient to identify a difference between the zero-force trajectories in different conditions.

Variability of hand speed.

To quantify the variability of hand speed, the crank velocity data from all trials within a speed and direction condition were binned into 200 position bins. In each bin, the coefficient of variation (CV) of hand speed was computed (standard deviation divided by the mean). Then the average of this metric across bins served as the second dependent measure for statistical analysis.

Statistical Analysis

All statistics were performed in MATLAB (v. 2022 b, The MathWorks, Natick, MA). To quantify the influence of speed and direction, a linear mixed model was used; it was then tested using analysis of variance (ANOVA). The linear model, which represented the observed dependent measure $Y_{i,j,k}$, was expressed as

$$Y_{i,j,k} = \mu_T + \alpha_j + \beta_k + \gamma_l + (\alpha\beta)_{j,k} + (\alpha\gamma)_{j,l} + (\beta\gamma)_{k,l} + (\alpha\beta\gamma)_{j,k,l} + E_{i,(j,k,l)} \quad (6)$$

where the grand mean is μ_T, the fixed effect of speed is α_j, where j is an index from 1 to 3, the fixed effect of direction is β_k, where k is an index from 1 to 2, and the random effect of subject is γ_l, where l is an index from 1 to 10. For the first dependent measure, $\ln(r)_{PC}$, the stochastic sampling effect was $E_{i,j,k}$, where i is an index from 1 to 22 (representing the number of trials excluding the first trials and the 7 catch trials). For the second dependent measure, the CV of speed, the index i was 1. This was because computing the CV over bins included all individual trials. The significance level was set to 5% for all statistical tests. Paired sample t tests were carried out to further interpret the results of the ANOVA. Significance values of post hoc tests were adjusted using the Šídák–Bonferroni procedure, where the original significance level was defined as $\alpha = 0.05$, the number of t tests was m, and the corrected Šídák–Bonferroni significance values were: $\alpha_{SID} = 1 - (1 - \alpha)^{1/m}$.

RESULTS

Variation of Force and Motion

Despite instructions and the availability of continuous visual feedback, movement speed fluctuated, displaying a systematic pattern with respect to crank angle in all three speed conditions (see Fig. 3). At the same time, the force normal to the constraint was also nonzero, again displaying a systematic pattern with respect to crank angle. To explore the possible cause of these patterns, we combined these observations by computing the zero-force trajectories.

Downloaded from journals.physiology.org/journal/jn at EPFL Bibliotheque USD (128.179.253.225) on January 16, 2024.

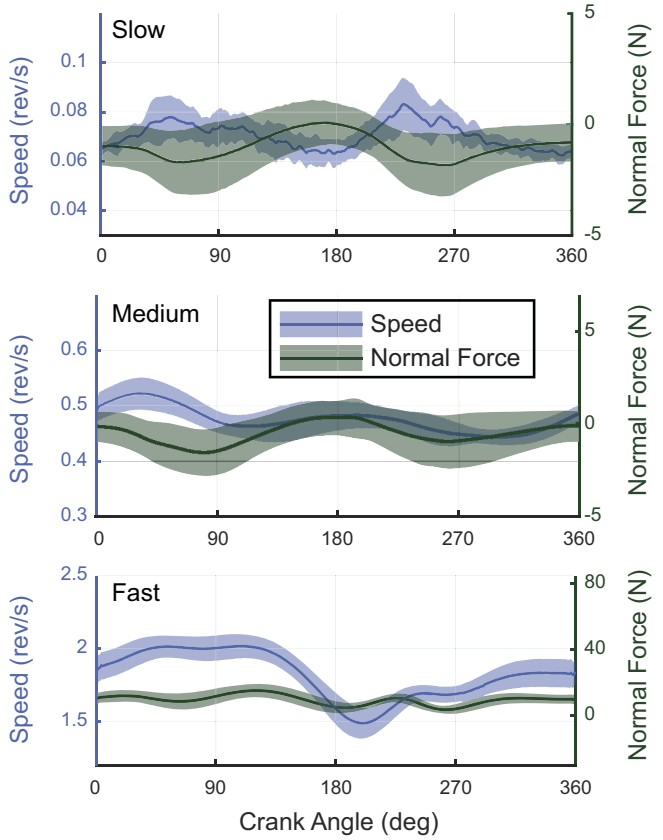

Figure 3. Mean and standard deviations of hand speed (blue solid line) and normal force (green solid line) versus crank angle for all subjects. The shading indicates 1 standard deviation from the mean. Data are from the clockwise (CW) direction trials. Systematic fluctuations in speed and force were observed with respect to crank position. Note the different scales on the ordinates.

Zero-Force Trajectory Orientation

A zero-force trajectory from one representative subject in each direction and speed condition is presented in Fig. 4. To provide a sense of the data across all subjects, the average zero-force trajectory for each subject binned by position, in each direction and speed condition, is presented in Fig. 5. From these two figures, it is clear that *1*) the trajectories were approximately elliptical for all three speeds, although to a varying degree; *2*) the shapes displayed a clear difference of orientation between the two directions; and *3*) there was a consistent pattern of speed fluctuations along the path with respect to crank position.

To quantify this difference in ellipse orientation, the ellipse was quantified by parameters in log-ratio coordinates (see METHODS) and presented in Fig. 6. Despite the variability of the data, the difference between CW and CCW directions is visually evident. The mean ± SD of $\ln(r)_{PC}$ in the CW conditions were 0.098 ± 0.12 (slow), 0.23 ± 0.15 (medium), and 0.58 ± 0.07 (fast) and in the CCW conditions were −0.21 ± 0.16 (slow), −0.27 ± 0.19 (medium), and −0.45 ± 0.09 (fast).

The parameter averages of $\ln(r)_{PC}$ are displayed in Fig. 6 (*bottom left*). Statistical analysis of $\ln(r)_{PC}$ revealed a significant interaction between speed and direction ($F_{2.0,18.0}$ = 106.388, $P < 0.001$) together with a main effect of speed ($F_{2.0,9.0}$ = 6.062, P = 0.006), and direction ($F_{1.0,9.0}$ = 212.879, $P < 0.001$). For each speed, post hoc pairwise t tests were performed between the CW and CCW directions. A significant difference between directions was observed in all three cases: slow ($P < 0.001$, $\alpha_{SID} = 0.017$), medium ($P < 0.001$, $\alpha_{SID} = 0.017$), and fast ($P < 0.001$, $\alpha_{SID} = 0.017$).

The original data are displayed in the lower left of Fig. 6. To clarify the effect of direction, the CCW data were reflected along the $\ln(r)_{PC}$ in the lower right figure. After reflection, a significant main effect of speed ($F_{2.0,9.0} = 106.388$, $P < 0.001$) and a significant interaction between speed and direction ($F_{2.0,18.0} = 6.0622$, $P = 0.006$) were detected. This reflection of the CCW about the $\ln(r_0)$ and $\ln(r_{45})$ axes showed the similarity of behavior in both CW and CCW directions. These results support *hypothesis 1*.

Orientation—Sensitivity Analysis

The zero-force trajectory is a construct derived from our experimental observations based on several assumptions combined with parameter values from the published literature. To assess the sensitivity of this construct to the assumptions used to compute it, key parameters of the model were varied over a 3:1 range. A linear time-invariant first-order model of mechanical impedance was assumed, with damping proportional to the assumed stiffness. Values for the gain term G were [0.25, 0.50, 0.75] (slow and medium), and [0.75, 1.50, 2.25] (fast); values of the proportionality constant β were [0.025 s, 0.05 s, 0.075 s] (slow and medium), and [0.05 s, 0.1 s, 0.15 s] (fast). As anticipated, when the impedance was varied, the zero-force trajectory changed. Nevertheless, the differences in ellipse orientation between conditions remained when the impedance parameters were varied (see Fig. 7). Hence, the orientation of the zero-force trajectory was not sensitive to the particular values of stiffness and damping; the observed results were robust.

Variability of Hand Speed

The variability of hand speed, measured by the coefficient of variation CV, is presented in Fig. 8. Hand speed variability was significantly higher at the slow speed compared with the faster two speeds. Statistically, the mean CV in the CW conditions was 0.26 ± 0.06 (slow), 0.13 ± 0.02 (medium), and 0.11 ± 0.03 (fast). The mean CV in the CCW conditions was 0.28 ± 0.06 (slow), 0.16 ± 0.02 (medium), and 0.11 ± 0.02 (fast). A significant interaction between speed and direction ($F_{2.0,18.0}$ = 3.489, $P < 0.038$) together with a main effect of speed ($F_{2.0,9.0}$ = 116.076, $P < 0.001$) and direction ($F_{1.0,9.0}$ = 5.755, $P < 0.014$) were detected. Note that the effects of direction and the interaction, though significant, were visibly weaker than the influence of speed. For each direction, post hoc pairwise t tests were performed between adjacent speeds. A significant difference was detected between the slow and medium speed for both CW ($P < 0.001$, $\alpha_{SID} = 0.013$) and CCW ($P < 0.001$, $\alpha_{SID} = 0.013$) directions. A significant difference was also detected between the medium and fast speeds in the CW ($P = 0.003$, $\alpha_{SID} = 0.013$) and CCW directions ($P < 0.001$, $\alpha_{SID} = 0.013$).

Downloaded from journals.physiology.org/journal/jn at EPFL Bibliotheque USD (128.179.253.225) on January 16, 2024.

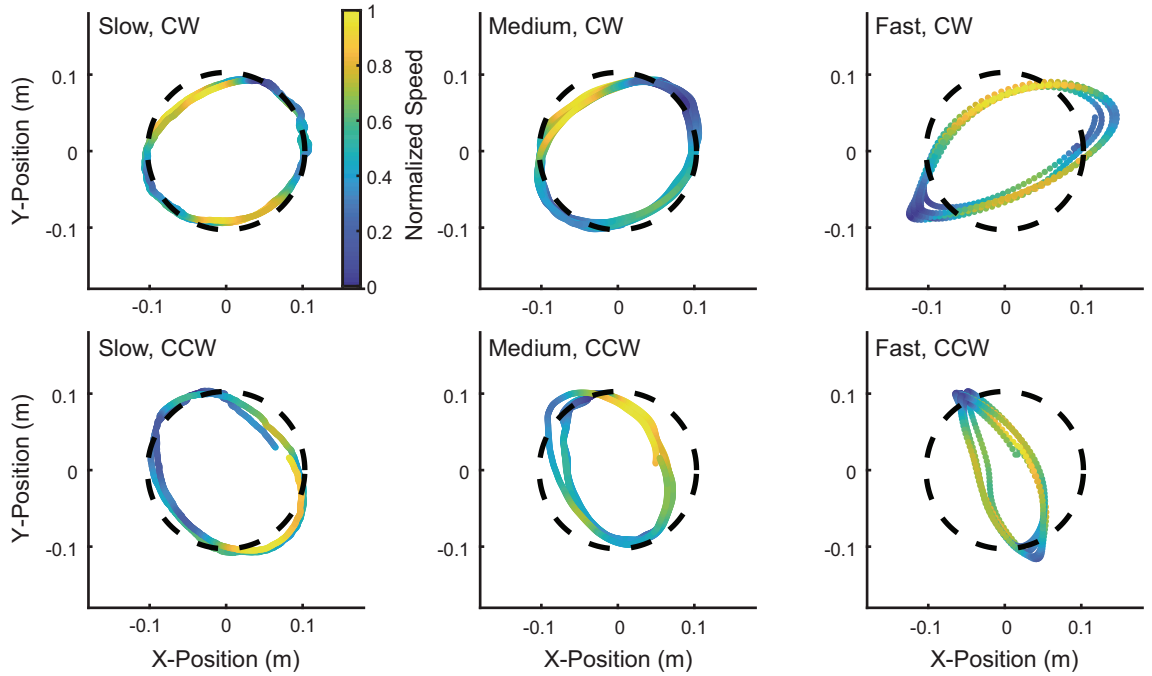

Figure 4. One representative trial from one subject in the slow, medium, and fast speed conditions (from left to right). *Top*: clockwise direction trials (CW); *bottom*: counterclockwise direction trials (CCW). The paths defined by the constraint are shown by the black dashed circle. The zero-force trajectories are shown by lines with varying color that indicates speed along the zero-force path (normalized by its range). Importantly, the zero-force trajectory is roughly elliptical for all speeds and its orientation differs with direction.

DISCUSSION

Kinematically constrained motion presents an intermediate step between widely studied unconstrained motions, such as reaching and pointing, and sparsely studied physical interaction with dynamically complex objects. Several works have investigated crank turning from a variety of perspectives including early descriptive studies (65), optimal control studies with muscle-level modeling (66–70), studies that investigated minimizing muscular effort (71), or summarized muscle behavior as an

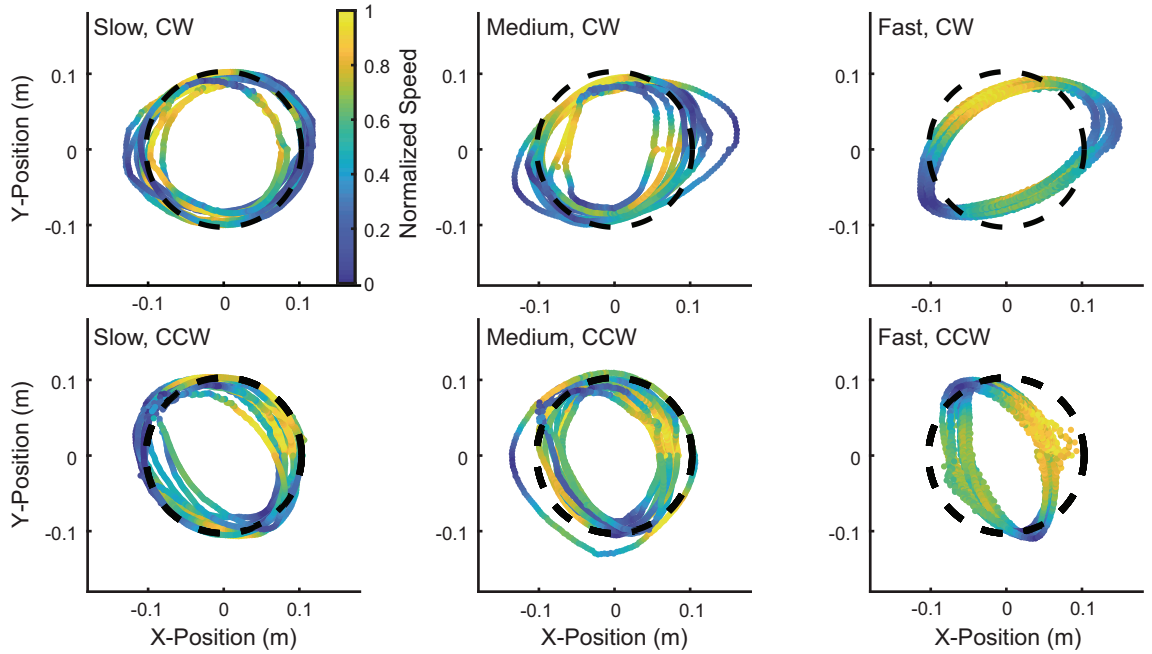

Figure 5. The average zero-force trajectories binned over angular position for each of the 10 subjects in the slow, medium, and fast speed conditions (from left to right). *Top*: clockwise direction trials (CW); *bottom*: counterclockwise direction trials (CCW). The path defined by the constraint is shown by the black dashed circle. The zero-force trajectories are shown by lines with varying color that indicates speed along the zero-force path (normalized by its range).

Downloaded from journals.physiology.org/journal/jn at EPFL Bibliotheque USD (128.179.253.225) on January 16, 2024.

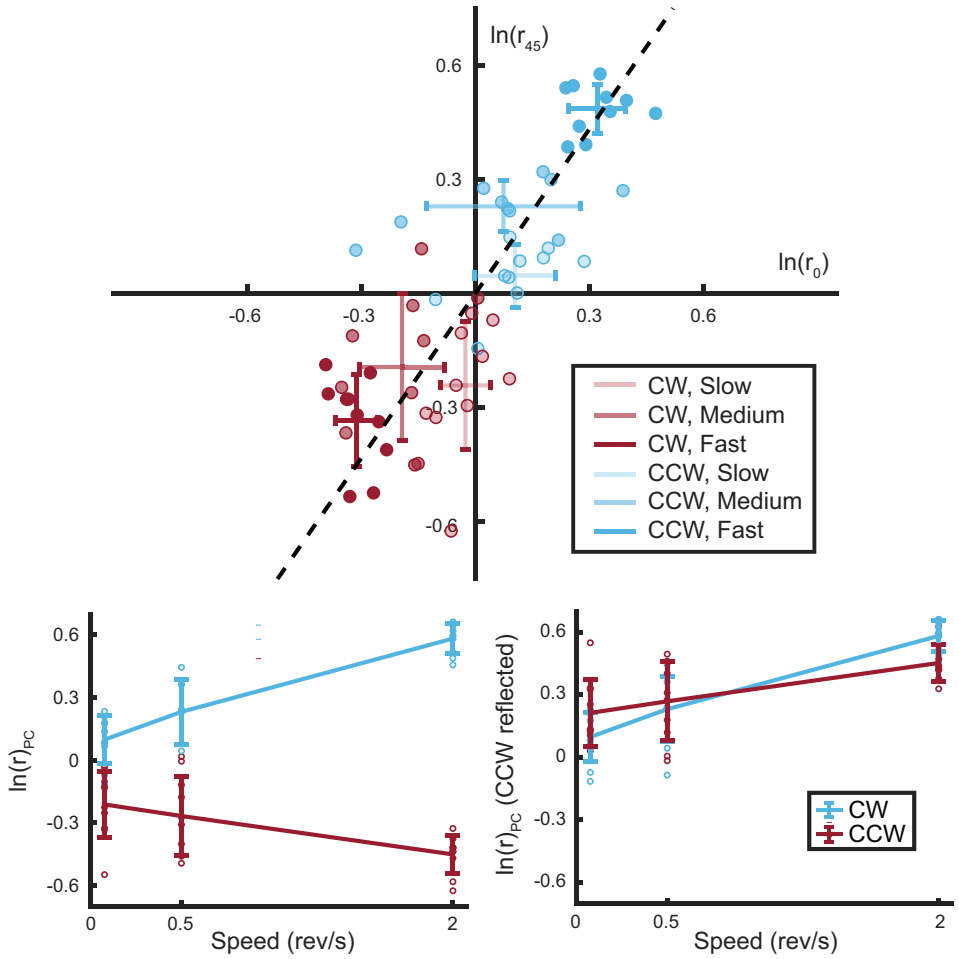

Figure 6. Distribution of ellipse parameters in ln(ratio) space. The clockwise (CW) direction is represented by blue, and the counterclockwise (CCW) direction is represented by red. Lighter shades indicate slower speeds and darker shades indicate faster speeds. The crosses represent plus or minus one standard deviation from the mean across subjects. The black dashed line represents the direction of the first principal component. *Bottom left*: distribution of dependent measure $\ln(r)_{PC}$ for the three speed conditions and two turning directions. Note the clear difference between the CW and CCW directions. *Bottom right*: the same distribution of the dependent measure $\ln(r)_{PC}$ but with CCW data reflected across the zero line.

impedance (21, 35), studies that looked at bicycle pedaling (72), as well as studies in robotics that tested different controllers for these task demands (73, 74).

A Single Measure of Force and Motion Control: The Zero-Force Trajectory

To understand the interaction with a kinematic constraint, our approach was to estimate an underlying zero-force trajectory. The zero-force trajectory is a construct based on measured force and motion, combined in a model of peripheral neuromechanics. It allows us to "peel back" the peripheral neuromechanics to uncover one consequence of the underlying neural commands; that consequence is expressed in terms of motion. The zero-force trajectory is similar to, but distinct from, the virtual trajectory of the equilibrium-point hypothesis (75–77). The virtual trajectory was postulated to be encoded in neural commands descending from the higher CNS to the periphery. However, the forward-path dynamics from the neural input to

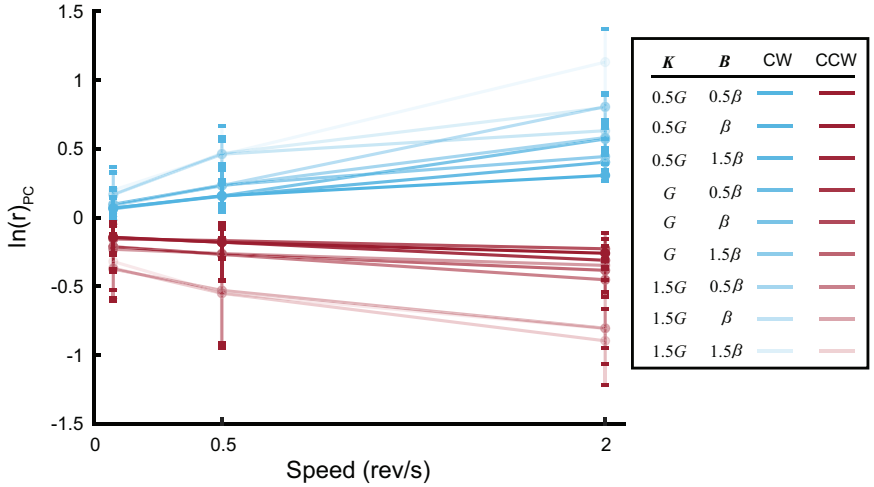

Figure 7. Distributions of the dependent measures $\ln(r)_{PC}$ for each speed when the impedance parameters were varied over a 3:1 range. Error bars indicate the standard deviation between subjects. Lighter shades indicate lower stiffness and damping and darker shades indicate higher stiffness and damping.

Downloaded from journals.physiology.org/journal/jn at EPFL Bibliotheque USD (128.179.253.225) on January 16, 2024.

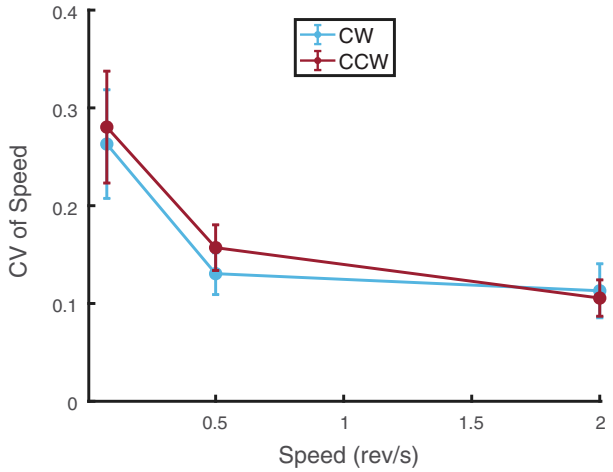

Figure 8. Coefficient of variation (CV) of hand speed for the different movement speeds. Error bars indicate the standard deviations between subjects. Blue lines indicate the clockwise trials (CW), red lines indicate the counterclockwise trials (CCW).

the actual motion is, in general, quite different from the interactive dynamics (mechanical impedance) used to construct the zero-force trajectory. For example, the classical paper by Gasser and Hill (78) showed that interactive behavior, characterized by a muscle's response to abrupt shortening, exhibited first-order dynamics. In contrast, the forward-path dynamics of muscle, typically characterized by its isometric twitch response to electrical stimulation of an alpha motoneuron, exhibits dynamics of at least second order (79). Because of differences in neural transmission delays and other dynamic effects (e.g., excitation-contraction coupling) between forward-path dynamics and interactive dynamics, the zero-force trajectory may differ substantially from the virtual trajectory. That was the main finding of the study by Gribble et al. (80). The zero-force trajectory is an objective observation defined by measurements of hand force and motion, combined with an experimental estimate of interactive dynamics. In combination with a reasonable model of peripheral neuromechanics, the zero-force trajectory is a way to interpret measured force and motion.

This study revealed a statistically significant difference in orientation of the zero-force trajectory between the CW and the CCW conditions, consistent with *hypothesis 1*. The rationale behind this hypothesis was that turning a crank with a two-joint arm might be executed using oscillatory primitives. Constant-speed circular hand motion requires sinusoidal motion in orthogonal directions with a phase offset of ±90° (depending on direction, CW vs. CCW). However, the oscillatory zero-force trajectory required to produce this motion would have to lead hand motion by an extent determined by the slow dynamic response of the neuromechanical periphery interacting with the inertia of the skeleton. That lead in time would manifest as a lead in phase that differed in opposite turning directions, and that would result in different performance in CW and CCW crank turning, just as we observed.

Consider a zero-force trajectory with two orthogonal components, x_0 and y_0, constructed from two out-of-phase sinusoids with the same frequency, Ω, same magnitude A, and a phase difference, ϕ

$$\begin{cases} x_0 = A\sin(\Omega t) \\ y_0 = A\sin(\Omega t + \phi) \end{cases} \quad (7)$$

A perfect circle can be drawn in the CW or CCW direction with a phase difference of ±90° (see APPENDIX C). However, slow peripheral neuromuscular dynamics interacting with skeletal inertia would require the zero-force trajectory to move ahead of the actual trajectory, contributing an additional phase difference. Moreover, because of the anisotropy of skeletal inertia and neuromuscular impedance, the magnitudes of the two sinusoidal components of the zero-force trajectory would differ. This would result in zero-force trajectories with elliptical shapes that are oriented differently for CW and CCW motions—just as we observed. The medium and fast speed behaviors strongly support this argument, implying that control may use oscillatory primitives.

Variability of Hand Speed: Evidence for Submovements

In our experiment, the standard deviation of hand speed declined monotonically with turning speed, being smallest at the slowest speed (21). However, while the coefficient of variation of hand speed was largely similar between the fast and medium speeds (both with periods less than 2 s), it increased significantly at the slowest speed (period of 13.3 s). For more than 100 years, researchers have documented movement intermittency, the inability to move smoothly and continuously during slow cyclical movements (13, 81), slow discrete movements (33, 82–85), goal-directed movements (86), and saccadic eye movements (87). In addition, studies with patients with stroke during rehabilitation have documented "fragmented" movements composed of highly stereotyped submovements (88, 89). This is vastly different from comfortably paced human reaching movements, which are usually smooth and follow a minimum-jerk trajectory (90). Consistent with these previous findings, the increased variability in the current trajectories likely reflects the emergence of component movements, or submovements.

An oscillation could, in theory, be a composite of opposite-direction submovements. However, physiological evidence indicates that this is not the case (36, 91). A well-documented observation in human psychology and motor control is that when the period of a rhythmic action[3] is longer than 2 to 5 s, it can no longer be perceived nor executed as periodic (55, 56). Slower movements, even if periodic, "break down" into a sequence of stereotyped submovements (33). These submovements may have limitations, e.g., amplitude, duration, and a minimum "refractory period"—time between initiation of adjacent submovements. Production of constant speed motion, with intermittent control, would require submovements to overlap (92, 93). As movement slows, the refractory period and minimum submovement duration make constant-speed motion impossible and individual submovement peaks appear. This causes greater variability at slow speeds, a quantifiable limitation of human behavior that may account for the increased fluctuations we observed in the slow-motion condition.

[3]In this context, consistent with the definitions in Refs. 48 and 49, "rhythmic" is a category encompassing several variations and degrees of strict periodicity.

Downloaded from journals.physiology.org/journal/jn at EPFL Bibliotheque USD (128.179.253.225) on January 16, 2024.

Limitations

The zero-force trajectory is an estimate based on a number of assumptions. It assumes a model of neuromuscular dynamics that is *1*) time-invariant, *2*) first-order, and *3*) linear. All of these assumptions are demonstrably incorrect, but they serve as a first workable approximation. The analysis also assumes that stiffness and damping are *1*) connected with a specific topology,[4] *2*) symmetric, and *3*) proportional, and *4*) that the same values of stiffness and damping may be applied to all subjects. Given the highly approximate nature of these assumptions, the regularity of the patterns that emerged is striking. Unlike Gomi and Kowato (94) showed for a reaching movement, the path of the zero-force trajectory that emerged in this study is "close" to the actual hand path. In particular, the effect of turning direction was observed even when the parameter G and the relative magnitude β of stiffness and damping were each varied over a 3:1 range.

One aspect of the assumed topology worth emphasizing is that the neuromuscular mechanical impedance has a well-defined zero. That allows the apparent behavior to be described as a Norton equivalent network. The Norton equivalent network is agnostic as to whether the apparent impedance results from a complete or a partial contribution from intrinsic biomechanics or neural feedback such as reflexes (53).

Experimentally, Mussa-Ivaldi et al. (58) observed that a constant joint space stiffness provided a good approximation of the variation of hand stiffness with limb configuration. In this work, a constant joint space stiffness was used to estimate the zero-force trajectory. Note that, by definition, a stiffness that depends only on configuration (and not motion) results in the same stiffness at each crank position regardless of turning direction. Furthermore, the inertial model was the same in both directions and cannot account for the observed differences (21).

Prior investigations have extracted submovements from free reaching movements with relatively short durations (33, 95–98). Others have examined tasks with longer durations, but assumed more structure, e.g., durations and onset times of the fitted basis function location (92). This work did not extract submovements from the zero-force trajectory estimates because without knowing the parameters of each submovement a priori for long data sets, the problem is computationally ill-posed. Furthermore, in the experiment, there was no evidence of stopping, not even in the slow case, making the identification of submovements challenging. The assumption of basis function, onset time, in combination with impedance parameters needed for this analysis were beyond what we could reasonably justify. Therefore, submovements were only discussed in the quasi-static case, which was too slow for oscillatory control.

Implications for an Account by Dynamic Primitives

While our observations are consistent with control based on a composition of underlying oscillations and submovements, we cannot rule out alternative explanations. Moreover, while we refer to these as dynamic primitives, we provide no direct evidence of their dynamic nature. A zero-force trajectory composed of oscillations and/or submovements provides a parsimonious, even elegant account of our observations. The zero-force trajectory is a coherent explanation of substantially nonzero normal forces, even though they did not contribute to mechanical work. It shows that patterns of force and velocity are clear with respect to configuration, but not time.

While our results are consistent with dynamic primitives in the production of kinematically constrained motions, they also presented a puzzle. Very slow speed behavior cannot be executed by oscillatory dynamic primitives, yet even the slow condition exhibited a feature easily explained by oscillatory primitives—direction dependence. The slowest speed, 13.33 s per revolution was quasi-static by any reasonable definition of the term (21). In that case, all inertial effects were negligible, as were any delays in the neuromuscular dynamics. What might account for the observed direction dependence at the slowest speed? One possibility is that the CNS develops some form of geometric representation of the behavior and uses it to generate a nominal slow-speed zero-force trajectory that serves as a target for feedback correction. Combined with an error threshold below which no action is taken, this may result in intermittent control, manifest as a sequence of submovements and resulting in an elevated coefficient of variation of hand speed (33, 92). The validity of these speculations is a topic for future study.

The existence of dynamic primitives does not preclude further organization or simplification at higher levels. However, higher-level goals may be constrained by these lower-level primitives. This may explain why humans do not globally minimize energy during crank turning (71) and why they fall into a rhythm, even when trying to hit a target in a sequence of throws (99).

Conclusions

This study examined kinematically constrained motion as an intermediate step to bridge the gap between unconstrained motions and physical interaction with dynamically complex objects. We investigated the detailed patterns of motion and force that human subjects exhibited when performing a simple constrained-motion task, turning a circular crank. Turning the crank in both CW and CCW directions at different speeds exposed several "artifacts" that could not result from mechanics alone. The zero-force trajectory displayed clear differences in orientation when turning in different directions. This is consistent with control using oscillatory primitives to generate an elliptical zero-force trajectory. However, when the oscillation period became longer than 2 to 5 s, motion became highly variable, probably giving rise to submovements. This reinforces previous observations (33) of a transition from smoothly rhythmic to intermittent control as actions slow.

Using dynamic primitives may allow humans to "work around" the shortcomings of their slow muscles and neural communication to perform complex physical interaction tasks. However, the advantages of this approach imply concomitant disadvantages. An elliptical zero-force trajectory that does not coincide with the circular constraint results in nonzero normal force applied to the crank (21). This was observed even at the slowest speed when dynamic

[4]In this context, "topology" refers to how the stiffness and damping are connected in the model. See APPENDIX D for discussion.

Downloaded from journals.physiology.org/journal/jn at EPFL Bibliotheque USD (128.179.253.225) on January 16, 2024.

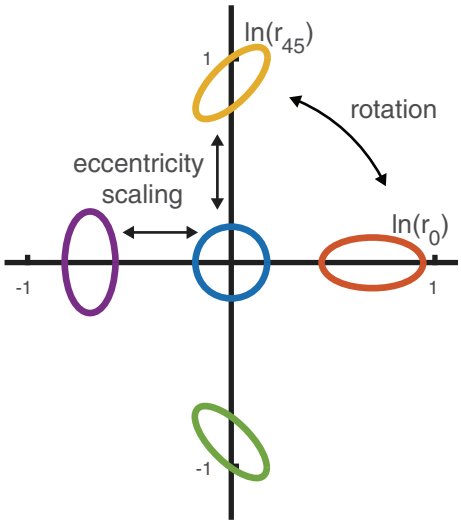

Figure A1. Graphical illustration of how the log-ratio coordinates change as the ellipse varies. The magnitude of the vector $[\ln(r_0), \ln(r_{45})]^T$ varies with ellipse eccentricity while its direction varies with major axis orientation.

effects were negligible and there was ample opportunity for feedback correction. This reinforces recent reports that human subjects interacting with a robot cannot suppress a dependence of interaction force on motion, even with visual feedback and opportunity to practice and learn (22, 100, 101). These limitations are important to understand the interaction between humans and the devices we develop, from complex robotic systems to simple handheld tools.

APPENDIX A: COORDINATE CHOICE

The ratio of major to minor axis lengths of the zero-force trajectory, especially in the slow condition, approached values close to unity (Fig. A1). When eccentricity is unity, the major axis orientation is not defined uniquely. For eccentricity close to unity, the distribution of major axis orientation is relatively flat and spread over a wide range of angles. This was the primary motivation for using the log-ratio coordinates. Figure A1 illustrates how the less intuitive log-ratio coordinates correspond to ellipse shape and orientation. The key point presented in Fig. A1 is that the magnitude of the vector $[\ln(r_0), \ln(r_{45})]^T$ varies with ellipse eccentricity while its direction varies with major axis orientation. The choice of log-ratio coordinates allowed investigation of slow conditions, a case where several subjects produced zero-force trajectories with an eccentricity close to unity. This was not previously possible when the eccentricity and major axis orientation coordinates were used (35).

APPENDIX B: MODELING A TWO-LINK MANIPULATOR COUPLED TO A CRANK

The arm was modeled as a two-link planar serial linkage, with no gravitational or frictional effects. Inertial parameters were estimated based on the cadaver studies of Dempster (102, 103). The shoulder joint was located at the thorax, which was assumed to be stationary. The model of the arm and crank system was constructed in the same manner as in Ref. 68. Model details including subject-specific inertial parameters are presented in the appendices of Ref. 21. Figure A2 displays the variables and notation used in the development of the model. The system has one degree of freedom; therefore, there is always a kinematic relation to transform from Cartesian position, $\boldsymbol{x} = [x, y]^T$, to joint position, $\boldsymbol{q} = [q_1, q_2]^T$, and to crank position, θ, where the center of the crank was defined as $\boldsymbol{x}_c = [x_c, y_c]$.

$$\boldsymbol{x} = \begin{bmatrix} l_1C_1 + l_2C_{12} \\ l_1S_1 + l_2S_{12} \end{bmatrix} = \begin{bmatrix} r\cos\theta \\ r\sin\theta \end{bmatrix} + \boldsymbol{x}_c \tag{8}$$

The notations S_1, C_1 denote $\sin(q_1)$, $\cos(q_1)$, and S_{12}, C_{12} denote $\sin(q_1 + q_2)$, $\cos(q_1 + q_2)$. The radius of the crank is r, the damping of the crank is b_c, and the inertia is I. The upper arm is denoted by 1, and the forearm denoted by 2 are described by length l_1, l_2, mass m_1, m_2, inertia about the z axis I_1, I_2, and center of mass distance from the joint axis c_1, c_2. The force on the handle is $\boldsymbol{F} = [F_x, F_y]^T$, with the normal unit vector, $\boldsymbol{n}$ and tangential unit vector, $\boldsymbol{e}$. The joint torque is denoted by $\tau = [\tau_1, \tau_2]^T$. The crank velocity is denoted $\dot{\theta}$ and the crank acceleration is denoted $\ddot{\theta}$.

From the sum of moments acting on the crank,

$$I\ddot{\theta} + b_c\dot{\theta} = r\boldsymbol{e}^T\boldsymbol{F} \tag{9}$$

summation of moments about the shoulder,

$$\boldsymbol{M}\ddot{\boldsymbol{q}} + \boldsymbol{h} = \tau - \boldsymbol{J}^T\boldsymbol{F} \tag{10}$$

and the kinematic relation that equates the acceleration at the handle to the acceleration at the hand,

$$\ddot{\boldsymbol{x}} = \boldsymbol{J}\ddot{\boldsymbol{q}} + \dot{\boldsymbol{J}}\dot{\boldsymbol{q}} = r(\ddot{\theta}\boldsymbol{e} - \dot{\theta}^2\boldsymbol{n}) \tag{11}$$

a model of the system could be constructed. Parameters comprising these equations include the mass matrix of a two-link manipulator $\boldsymbol{M}(\boldsymbol{q})$, the centrifugal and Coriolis forces $\boldsymbol{h}(\boldsymbol{q}, \dot{\boldsymbol{q}})$, and the Jacobian relating unconstrained differential arm motions to hand motions, $\boldsymbol{J}(\boldsymbol{q})$.

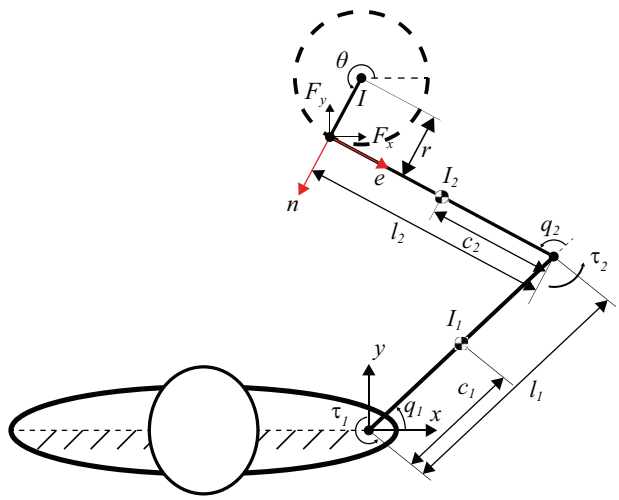

Figure A2. Model of crank rotation task that displays the sign convention and notation used in the computations.

Downloaded from journals.physiology.org/journal/jn at EPFL Bibliotheque USD (128.179.253.225) on January 16, 2024.

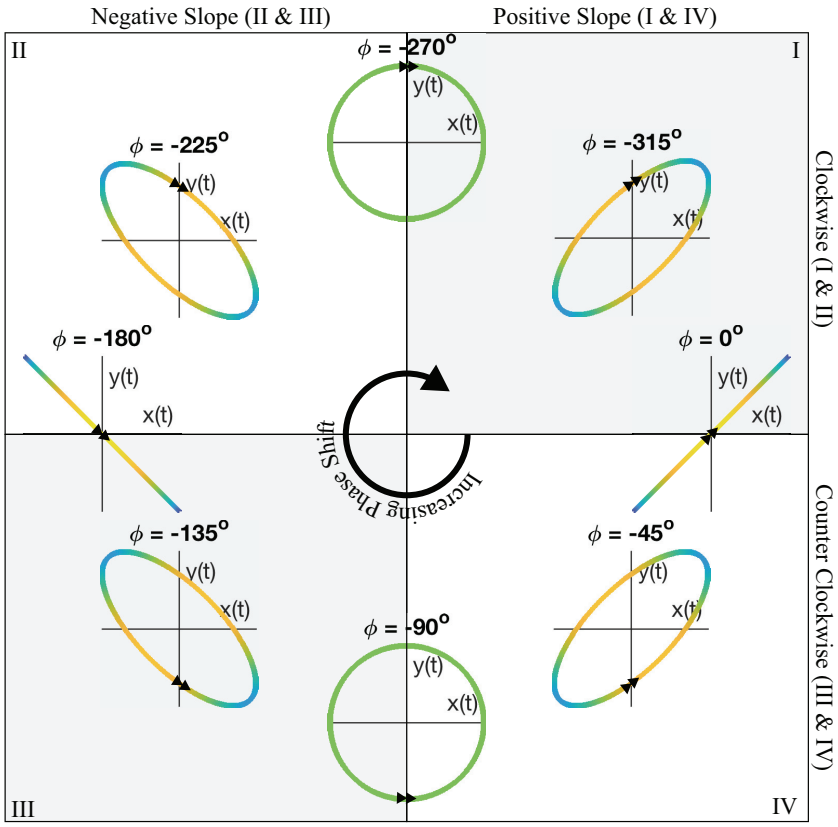

Figure A3. Trajectories resulting from two sinusoids in orthogonal orientation that are out of phase. To draw a perfect circle, a ±90° phase shift is required, with the sign depending on the direction, clockwise (CW) or counterclockwise (CCW). However, the limb dynamics add phase, thus different zero-force trajectories in the III and II quadrants are observed for the CW and CCW directions, respectively. This figure is replicated from Al-Khazali et al. (104).

APPENDIX C: ELLIPSE PHASE

Trajectories resulting from two sinusoids in orthogonal orientation are shown in a so-called Lissajous plot. The ellipse resulting from changing the phase between two sinusoids with the same amplitude and frequency are displayed in Fig. A3. To draw a perfect circle, a ±90° phase shift between the two sinusoids is required, with the sign generating different directions (denoted by black arrows in Fig. A3), CW or CCW. However, the limb dynamics add phase, thus different zero-force trajectories as in the II and III quadrants are observed for the CW and CCW directions, respectively.

APPENDIX D: TOPOLOGY

A model of upper-limb impedance often includes a stiffness and a damping term. However, unlike stiffness, which is usually defined as a displacement relative to the zero-force trajectory, damping can be defined relative to either the zero-force trajectory or to a constant velocity, often zero. The choice of this reference fundamentally changes the transfer function. Consider two simple linear mass spring damper systems. With damping relative to zero velocity,

$$m\ddot{x} = k(x_0 - x) + b\dot{x} \tag{12}$$

we can take the Laplace transform and solve for the transfer function,

$$\frac{X(s)}{X_0(s)} = \frac{k}{ms^2 + bs + k} \tag{13}$$

With damping relative to the zero-force trajectory, velocity is displayed graphically in Fig. 3. From the equation of motion,

$$m\ddot{x} = k(x_0 - x) + b(\dot{x}_0 - \dot{x}) \tag{14}$$

we can take the Laplace transform and solve for the transfer function,

$$\frac{X(s)}{X_0(s)} = \frac{bs + k}{ms^2 + bs + k} \tag{15}$$

To the extent that apparent neuromuscular mechanical impedance arises from muscle mechanics and/or reflex feedback, it cannot be referenced to any "nonlocal" variable, it must be referenced to a nominal neurally defined motion, not to "ground." Furthermore, this example shows that when the damping is defined relative to the zero-force trajectory, a dynamic zero is added to the system. McIntyre and Bizzi (105) found that damping relative to the zero-force trajectory enhances the control-following ability of the limb during single-joint movements. In addition, muscle spindles actively provide feedback about a change in position and velocity of the muscle. Damping relative to the zero-force trajectory is consistent with muscle spindle physiology and was used in the subsequent calculations.

DATA AVAILABILITY

Code: https://www.doi.org/10.5281/zenodo.10059509. The code is also available on at github at: https://github.com/jameshermus/crankTurning-dynamicPrimitives.

Data: https://www.doi.org/10.5281/zenodo.10059389.

GRANTS

J. Hermus was supported in part by a Harrington Fellowship. D. Sternad was supported by NIH-R37-HD087089, NIH R01-HD087089, NIH-R01-CRCNS-NS120579, and NSF-M3X-1825942. N. Hogan was supported in part by the Eric P. and Evelyn E.

Downloaded from journals.physiology.org/journal/jn at EPFL Bibliotheque USD (128.179.253.225) on January 16, 2024.

Newman Fund, NSF-CRCNS-1724135, NSF-M3X-1826097, and NIH-R01-HD087089.

DISCLOSURES

No conflicts of interest, financial or otherwise, are declared by the authors.

AUTHOR CONTRIBUTIONS

J.H., J.D., and N.H. conceived and designed research; J.D. performed experiments; J.H. analyzed data; J.H., D.S., and N.H. interpreted results of experiments; J.H. prepared figures; J.H. drafted manuscript; J.H., D.S., and N.H. edited and revised manuscript; J.H., J.D., D.S., and N.H. approved final version of manuscript.

REFERENCES

1. **Kandel ER**, **Schwartz JH**, **Jessell TM**, **Siegelbaum SA**, **Hudspeth AJ (Editors).** *Principles of Neural Science* (5th ed.). New York: McGraw-Hill, 2013.
2. **Loram ID**, **Maganaris CN**, **Lakie M.** Human postural sway results from frequent, ballistic bias impulses by soleus and gastrocnemius. *J Physiol* 564: 295–311, 2005. doi:10.1113/jphysiol.2004.076307.
3. **Shepard RN**, **Metzler J.** Mental rotation of three-dimensional objects. *Science* 171: 701–703, 1971. doi:10.1126/science.171.3972.701.
4. **Faisal AA**, **Selen LPJ**, **Wolpert DM.** Noise in the nervous system. *Nat Rev Neurosci* 9: 292–303, 2008. doi:10.1038/nrn2258.
5. **Sternad D.** It's not (only) the mean that matters: variability, noise and exploration in skill learning. *Curr Opin Behav Sci* 20: 183–195, 2018. doi:10.1016/J.COBEHA.2018.01.004.
6. **Dingwell JB**, **Mah CD**, **Mussa-Ivaldi FA.** Manipulating objects with internal degrees of freedom: evidence for model-based control. *J Neurophysiol* 88: 222–235, 2002. doi:10.1152/jn.2002.88.1.222.
7. **Bazzi S**, **Sternad D.** Human manipulation of dynamically complex objects through control contraction metrics. *IEEE Robot Autom Lett* 5: 2578–2585, 2020. doi:10.1109/lra.2020.2972863.
8. **Maurice P**, **Hogan N**, **Sternad D.** Predictability, force, and (anti)resonance in complex object control. *J Neurophysiol* 120: 765–780, 2018. doi:10.1152/jn.00918.2017.
9. **Razavian RS**, **Sadeghi M**, **Bazzi S**, **Nayeem R**, **Sternad D.** Body mechanics, optimality, and sensory feedback in the human control of complex objects. *Neural Comput* 35: 853–895, 2023. doi:10.1162/NECO_A_01576.
10. **Petrich L**, **Jin J**, **Dehghan M**, **Jagersand M.** A quantitative analysis of activities of daily living: insights into improving functional independence with assistive robotics. *2022 International Conference on Robotics and Automation (ICRA).* Philadelphia, PA, 2022, p. 6999–7006.
11. **Fitts PM.** The information capacity of the human motor system in controlling the amplitude of movement. *J Exp Psychol* 47: 381–391, 1954. doi:10.1037/h0055392.
12. **Buchanan JJ**, **Park J-H**, **Shea CH.** Target width scaling in a repetitive aiming task: switching between cyclical and discrete units of action. *Exp Brain Res* 175: 710–725, 2006. doi:10.1007/s00221-006-0589-1.
13. **Crossman ER**, **Goodeve PJ.** Feedback control of hand-movement and Fitts' law. *Q J Exp Psychol A* 35: 251–278, 1983. doi:10.1080/14640748308402133.
14. **Guiard Y.** On Fitts's and Hooke's laws: simple harmonic movement in upper-limb cyclical aiming. *Acta Psychol (Amst)* 82: 139–159, 1993. doi:10.1016/0001-6918(93)90009-G.
15. **Lacquaniti F**, **Terzuolo C**, **Viviani P.** The law relating the kinematic and figural aspects of drawing movements. *Acta Psychol (Amst)* 54: 115–130, 1983. doi:10.1016/0001-6918(83)90027-6.
16. **Abend W**, **Bizzi E**, **Morasso P.** Human arm trajectory formation. *Brain* 105: 331–348, 1982. doi:10.1093/brain/105.2.331.
17. **Massey JT**, **Lurito JT**, **Pellizzer G**, **Georgopoulos AP.** Three-dimensional drawings in isometric conditions: relation between geometry and kinematics. *Exp Brain Res* 88: 685–690, 1992. doi:10.1007/BF00228198.
18. **Schaal S**, **Sternad D.** Origins and violations of the 2/3 power law in rhythmic three-dimensional arm movements. *Exp Brain Res* 136: 60–72, 2001. doi:10.1007/s002210000505.
19. **Schwartz AB.** Direct cortical representation of drawing. *Science* 265: 540–542, 1994. doi:10.1126/science.8036499.
20. **Chib VS**, **Krutky MA**, **Lynch KM**, **Mussa-Ivaldi FA.** The separate neural control of hand movements and contact forces. *J Neurosci* 29: 3939–3947, 2009. doi:10.1523/JNEUROSCI.5856-08.2009.
21. **Hermus J**, **Doeringer J**, **Sternad D**, **Hogan N.** Separating neural influences from peripheral mechanics: the speed-curvature relation in mechanically-constrained actions. *J Neurophysiol* 123: 1870–1885, 2020. doi:10.1152/jn.00536.2019.
22. **West AM Jr**, **Hermus J**, **Huber ME**, **Maurice P**, **Sternad D**, **Hogan N.** Dynamic primitives limit human force regulation during motion. *IEEE Robot Autom Lett* 7: 2391–2398, 2022. doi:10.1109/LRA.2022.3141778.
23. **Hogan N.** Impedance control: an approach to manipulation: part II—implementation. *J Dyn Syst Meas Control* 107: 8–16, 1985. doi:10.1115/1.3140713.
24. **Loeb GE**, **Brown IE**, **Cheng EJ.** A hierarchical foundation for models of sensorimotor control. *Exp Brain Res* 126: 1–18, 1999. doi:10.1007/S002210050712/METRICS.
25. **Lee H**, **Hogan N.** Time-varying ankle mechanical impedance during human locomotion. *IEEE Trans Neural Syst Rehabil Eng* 23: 755–764, 2015. doi:10.1109/TNSRE.2014.2346927.
26. **Kearney RE**, **Hunter IW.** System identification of human joint dynamics. *Crit Rev Biomed Eng* 18: 55–87, 1990.
27. **Bennett DJ**, **Hollerbach JM**, **Xu Y**, **Hunter IW.** Time-varying stiffness of human elbow joint during cyclic voluntary movement. *Exp Brain Res* 88: 433–442, 1992. doi:10.1007/BF02259118.
28. **Rouse EJ**, **Hargrove LJ**, **Perreault EJ**, **Peshkin MA**, **Kuiken TA.** Development of a mechatronic platform and validation of methods for estimating ankle stiffness during the stance phase of walking. *J Biomech Eng* 135: 81009, 2013. doi:10.1115/1.4024286.
29. **Perreault EJ**, **Kirsch RF**, **Acosta AM.** Multiple-input, multiple-output system identification for characterization of limb stiffness dynamics. *Biol Cybern* 80: 327–337, 1999. doi:10.1007/s004220050529.
30. **Van De Ruit M**, **Cavallo G**, **Lataire J**, **Van Der Helm FCT**, **Mugge W**, **Van Wingerden JW**, **Schouten AC.** Revealing time-varying joint impedance with kernel-based regression and nonparametric decomposition. *IEEE Trans Contr Syst Technol* 99: 1–14, 2018. doi:10.1109/TCST.2018.2881664.
31. **Wolpert DM**, **Kawato M.** Multiple paired forward and inverse models for motor control. *Neural Netw* 11: 1317–1329, 1998. doi:10.1016/S0893-6080(98)00066-5.
32. **Wolpert DM**, **Miall RC**, **Kawato M.** Internal models in the cerebellum. *Trends Cogn Sci* 2: 338–347, 1998. doi:10.1016/S1364-6613(98)01221-2.
33. **Park S-W**, **Marino H**, **Charles SK**, **Sternad D**, **Hogan N.** Moving slowly is hard for humans: limitations of dynamic primitives. *J Neurophysiol* 118: 69–83, 2017. doi:10.1152/jn.00643.2016.
34. **Nah MC**, **Krotov A**, **Russo M**, **Sternad D**, **Hogan N.** Dynamic primitives facilitate manipulating a whip. *2020 8th IEEE RAS/EMBS International Conference for Biomedical Robotics and Biomechatronics (BioRob).* New York, NY, 2020, p. 685–691. doi:10.1109/BioRob49111.2020.9224399.
35. **Hermus J**, **Sternad D**, **Hogan N.** Evidence for dynamic primitives in a constrained motion task. *2020 8th IEEE RAS/EMBS International Conference for Biomedical Robotics and Biomechatronics (BioRob).* New York, NY, 2020, p. 551–556. doi:10.1109/BioRob49111.2020.9224352.
36. **Schaal S**, **Sternad D**, **Osu R**, **Kawato M.** Rhythmic arm movement is not discrete. *Nat Neurosci* 7: 1136–1143, 2004. doi:10.1038/nn1322.
37. **Sternad D**, **Dean WJ**, **Schaal S.** Interaction of rhythmic and discrete pattern generators in single-joint movements. *Hum Mov Sci* 19: 627–664, 2000. doi:10.1016/S0167-9457(00)00028-2.
38. **Sternad D**, **Schaal S.** Segmentation of endpoint trajectories does not imply segmented control. *Exp Brain Res* 124: 118–136, 1999. doi:10.1007/s002210050606.
39. **Giszter SF.** Motor primitives — new data and future questions. *Curr Opin Neurobiol* 33: 156–165, 2015. doi:10.1016/j.conb.2015.04.004.

Downloaded from journals.physiology.org/journal/jn at EPFL Bibliotheque USD (128.179.253.225) on January 16, 2024.

40. **Kargo WJ**, **Giszter SF.** Individual premotor drive pulses, not time-varying synergies, are the units of adjustment for limb trajectories constructed in spinal cord. *J Neurosci* 28: 2409–2425, 2008. doi:10.1523/JNEUROSCI.3229-07.2008.
41. **Bernstein N.** *The Coordination and Regulation of Movements*. Oxford, UK: Pergamon, 1967.
42. **d'Avella A**, **Saltiel P**, **Bizzi E.** Combinations of muscle synergies in the construction of a natural motor behavior. *Nat Neurosci* 6: 300–308, 2003. doi:10.1038/nn1010.
43. **Borghese NA**, **Bianchi L**, **Lacquaniti F.** Kinematic determinants of human locomotion. *J Physiol* 494: 863–879, 1996. doi:10.1113/JPHYSIOL.1996.SP021539.
44. **Doshi N**, **Hogan FR**, **Rodriguez A.** Hybrid differential dynamic programming for planar manipulation primitives (Preprint). *arXiv*, 2020. doi:10.48550/arXiv.1911.00175.
45. **Hogan FR**, **Ballester J**, **Dong S**, **Rodriguez A.** Tactile dexterity: manipulation primitives with tactile feedback (Preprint). *arXiv*, 2020. doi:10.48550/arXiv.2002.03236.
46. **Chavan-Dafle N**, **Rodriguez A.** Prehensile pushing: in-hand manipulation with push-primitives. *2015 IEEE/RSJ International Conference on Intelligent Robots and Systems (IROS)*. Hamburg, Germany, 2015, p. 6215–6222. doi:10.1109/IROS.2015.7354264.
47. **Hogan N.** Physical interaction via dynamic primitives. In: *Geometric and Numerical Foundations of Movements*, edited by Laumond J-P, Mansard N, Lasserre J-B. Cham, Switzerland: Springer, 2017, p. 269–299.
48. **Hogan N**, **Sternad D.** On rhythmic and discrete movements: reflections, definitions and implications for motor control. *Exp Brain Res* 181: 13–30, 2007. doi:10.1007/s00221-007-0899-y.
49. **Hogan N**, **Sternad D.** Dynamic primitives of motor behavior. *Biol Cybern* 106: 727–739, 2012. doi:10.1007/s00422-012-0527-1.
50. **Hogan N**, **Sternad D.** Dynamic primitives in the control of locomotion. *Front Comput Neurosci* 7: 71, 2013. doi:10.3389/fncom.2013.00071.
51. **Schaal S**, **Kotosaka S**, **Sternad D.** Nonlinear dynamical systems as movement primitives. *IEEE International Conference on Humanoid Robotics*, 2001, p. 1–11.
52. **de Rugy A**, **Sternad D.** Interaction between discrete and rhythmic movements: reaction time and phase of discrete movement initiation during oscillatory movements. *Brain Res* 994: 160–174, 2003. doi:10.1016/J.BRAINRES.2003.09.031.
53. **Hogan N.** A General Actuator Model Based on Nonlinear Equivalent Networks. *IEEE/ASME Trans Mechatron* 19: 1929–1939, 2014. doi:10.1109/TMECH.2013.2294096.
55. **James W.** *The Principles of Psychology*. New York: Henry Holt and Company, 1890.
56. **Fraisse P.** Perception and estimation of time. *Annu Rev Psychol* 35: 1–36, 1984. doi:10.1146/annurev.ps.35.020184.000245.
57. **Hogan N.** An organizing principle for a class of voluntary movements. *J Neurosci* 4: 2745–2754, 1984. doi:10.1523/JNEUROSCI.04-11-02745.1984.
58. **Mussa-Ivaldi FA**, **Hogan N**, **Bizzi E.** Neural, mechanical, and geometric factors subserving arm posture in humans. *J Neurosci* 5: 2732–2743, 1985. doi:10.1523/JNEUROSCI.05-10-02732.1985.
59. **Flash T.** The control of hand equilibrium trajectories in multi-joint arm movements. *Biol Cybern* 57: 257–274, 1987. doi:10.1007/BF00338819.
60. **Hill AV.** The heat of shortening and the dynamic constants of muscle. *Proc R Soc Lond B Biol Sci* 126: 136–195, 1938. doi:10.1098/rspb.1938.0050.
61. **Cannon SC**, **Zahalak GI.** The mechanical behavior of active human skeletal muscle in small oscillations. *J Biomech* 15: 111–121, 1982. doi:10.1016/0021-9290(82)90043-4.
62. **Lacquaniti F**, **Licata F**, **Soechting JF.** The mechanical behavior of the human forearm in response to transient perturbations. *Biol Cybern* 44: 35–46, 1982. doi:10.1007/BF00353954.
63. **Fasse ED**, **Hogan N.** Control of physical contact and dynamic interaction. In: *Robotics Research: The Seventh International Symposium*. London: Springer, 1996, p. 28–38.
64. **Fasse ED**, **Hogan N**, **Kay BA**, **Mussa-Ivaldi FA.** Haptic interaction with virtual objects. *Biol Cybern* 82: 69–83, 2000. doi:10.1007/PL00007962.
65. **Russell D**, **Hogan N.** Dealing with constraints: a biomechanical approach. In: *Images of the Twenty-First Century. Proceedings of the Annual International Engineering in Medicine and Biology Society*. Seattle, WA, 1989, p. 892–893, vol. 3. doi:10.1109/IEMBS.1989.96034.
66. **Svinin MM**, **Ohta K**, **Luo ZW**, **Hosoe S.** Understanding of human movements in crank rotation. *Proceedings 2001 IEEE/RSJ International Conference on Intelligent Robots and Systems. Expanding the Societal Role of Robotics in the Next Millennium (Cat. No.01CH37180)*. Maui, HI, 2001, p. 2105–2110, vol. 4. doi:10.1109/IROS.2001.976382.
67. **Ohta K**, **Luo Z-W**, **Ito M.** Analysis of human movement under environmental constraints: adaptability to environment during crank rotation tasks. *Transactions of the Institute of Electronics, Information and Communication Engineers* 81: 1392–1401, 1998.
68. **Ohta K**, **Svinin MM**, **Luo Z**, **Hosoe S**, **Laboissière R.** Optimal trajectory formation of constrained human arm reaching movements. *Biol Cybern* 91: 23–36, 2004. doi:10.1007/s00422-004-0491-5.
69. **Davoudabadi Farahani S**, **Svinin M**, **Andersen MS**, **de Zee M**, **Rasmussen J.** Prediction of closed-chain human arm dynamics in a crank-rotation task. *J Biomech* 49: 2684–2693, 2016. doi:10.1016/J.JBIOMECH.2016.05.034.
70. **Zheng Z**, **Wang R.** Arm motion control model based on central pattern generator. *Appl. Math Mech* 38: 1247–1256, 2017. doi:10.1007/S10483-017-2240-8.
71. **Koeppen R**, **Huber M**, **Sternad D**, **Hogan V.** Controlling physical interactions: humans do not minimize muscle effort. *Proc ASME Dyn Syst Control Conf* 2017: V001T36A003, 2017. doi:10.1115/DSCC2017-5202.
72. **Raasch CC**, **Zajac FE.** Locomotor strategy for pedaling: muscle groups and biomechanical functions. *J Neurophysiol* 82: 515–525, 1999. doi:10.1152/jn.1999.82.2.515.
73. **Williamson MM.** Oscillators and crank turning: exploiting natural dynamics with a humanoid robot arm. *Philos Trans A Math Phys Eng Sci* 361: 2207–2223, 2003. doi:10.1098/rsta.2003.1272.
74. **Kazanzides P**, **Bradley NS**, **Wolovich WA.** Dual-drive force/velocity control: Implementation and experimental results. *Proceedings, 1989 International Conference on Robotics and Automation*. Scottsdale, United States, 1989, p. 92–97. doi:10.1109/ROBOT.1989.99973.
75. **Bizzi E**, **Accornero N**, **Chapple W**, **Hogan N.** Arm trajectory formation in monkeys. *Exp Brain Res* 46: 139–143, 1982. doi:10.1007/BF00238107.
76. **Feldman AG.** Functional tuning of the nervous system during control of movement or maintenance of a steady posture. II. Controllable parameters of the muscles. *Biophysics (Oxf)* 11: 565–578, 1966.
77. **Feldman AG.** Once more on the equilibrium-point hypothesis (lambda model) for motor control. *J Mot Behav* 18: 17–54, 1986. doi:10.1080/00222895.1986.10735369.
78. **Gasser HS**, **Ill AVH.** The dynamics of muscular contraction. *Proc R Soc Lond B Biol Sci* 96: 398–437, 1924. doi:10.1098/RSPB.1924.0035.
79. **Van Bolhuis AI**, **Holsheimer J**, **Savelberg HHCM.** A nerve stimulation method to selectively recruit smaller motor-units in rat skeletal muscle. *J Neurosci Methods* 107: 87–92, 2001. doi:10.1016/S0165-0270(01)00355-7.
80. **Gribble PL**, **Ostry DJ**, **Sanguineti V**, **Laboissière R.** Are complex control signals required for human arm movement? *J Neurophysiol* 79: 1409–1424, 1998. doi:10.1152/jn.1998.79.3.1409.
81. **Doeringer JA**, **Hogan N.** Intermittency in preplanned elbow movements persists in the absence of visual feedback. *J Neurophysiol* 80: 1787–1799, 1998. doi:10.1152/jn.1998.80.4.1787.
82. **Hogan N**, **Doeringer JA**, **Krebs HI.** Arm movement control is both continuous and discrete. *Cognitive Studies* 6: 254–273, 1999. doi:10.11225/jcss.6.254.
83. **Vallbo AB**, **Wessberg J.** Organization of motor output in slow finger movements in man. *J Physiol* 469: 673–691, 1993. doi:10.1113/jphysiol.1993.sp019837.
84. **van der Wel RPRD**, **Sternad D**, **Rosenbaum DA.** Moving the arm at different rates: slow movements are avoided. *J Mot Behav* 42: 29–36, 2010. doi:10.1080/00222890903267116.
85. **Woodworth RS.** The accuracy of voluntary movements. *The Psychological Review* 3: i–114, 1899. doi:10.1037/h0092992.
86. **Milner TE.** A model for the generation of movements requiring endpoint precision. *Neuroscience* 49: 487–496, 1992. doi:10.1016/0306-4522(92)90113-G.
87. **Collewijn H**, **Erkelens CJ**, **Steinman RM.** Binocular co-ordination of human horizontal saccadic eye movements. *J Physiol* 404: 157–182, 1988. doi:10.1113/jphysiol.1988.sp017284.

Downloaded from journals.physiology.org/journal/jn at EPFL Bibliotheque USD (128.179.253.225) on January 16, 2024.

88. **Krebs HI**, **Aisen ML**, **Volpe BT**, **Hogan N.** Quantization of continuous arm movements in humans with brain injury. *Proc Natl Acad Sci USA* 96: 4645–4649, 1999. doi:10.1073/pnas.96.8.4645.
89. **Rohrer B**, **Fasoli S**, **Krebs HI**, **Volpe B**, **Frontera WR**, **Stein J**, **Hogan N.** Submovements grow larger, fewer, and more blended during stroke recovery. *Motor Control* 8: 472–483, 2004. doi:10.1123/mcj.8.4.472.
90. **Flash T**, **Hogan N.** The coordination of arm movements: an experimentally confirmed mathematical model. *J Neurosci* 5: 1688–1703, 1985. doi:10.1523/JNEUROSCI.05-07-01688.1985.
91. **Grillner S**, **Wallen P.** Central pattern generators for locomotion, with special reference to vertebrates. *Annu Rev Neurosci* 8: 233–261, 1985. doi:10.1146/annurev.ne.08.030185.001313.
92. **Markkula G**, **Boer E**, **Romano R**, **Merat N.** Sustained sensorimotor control as intermittent decisions about prediction errors: computational framework and application to ground vehicle steering. *Biol Cybern* 112: 181–207, 2018. doi:10.1007/s00422-017-0743-9.
93. **Loram ID**, **van de Kamp C**, **Lakie M**, **Gollee H**, **Gawthrop PJ.** Does the motor system need intermittent control? *Exerc Sport Sci Rev* 42: 117–125, 2014. doi:10.1249/jes.0000000000000018.
94. **Gomi H**, **Kawato M.** Equilibrium-point control hypothesis examined by measured arm stiffness during multijoint movement. *Science* 272: 117–120, 1996. doi:10.1126/science.272.5258.117.
95. **Rohrer B**, **Hogan N.** Avoiding spurious submovement decompositions: a globally optimal algorithm. *Biol Cybern* 89: 190–199, 2003. doi:10.1007/s00422-003-0428-4.
96. **Rohrer B**, **Hogan N.** Avoiding spurious submovement decompositions II: a scattershot algorithm. *Biol Cybern* 94: 409–414, 2006. doi:10.1007/s00422-006-0055-y.
97. **Plamondon R**, **Alimi AM**, **Yergeau P**, **Leclerc F.** Modelling velocity profiles of rapid movements: a comparative study. *Biol Cybern* 69: 119–128, 1993. doi:10.1007/BF00226195.
98. **Gowda S**, **Overduin SA**, **Chen M**, **Chang YH**, **Tomlin CJ**, **Carmena JM.** Accelerating submovement decomposition with search-space reduction heuristics. *IEEE Trans Biomed Eng* 62: 2508–2515, 2015. doi:10.1109/TBME.2015.2434595.
99. **Zhang Z**, **Sternad D.** The primacy of rhythm: how discrete actions merge into a stable rhythmic pattern. *J Neurophysiol* 121: 574–587, 2019. doi:10.1152/jn.00587.2018.
100. **Maurice P**, **Huber ME**, **Hogan N**, **Sternad D.** Velocity-curvature patterns limit human–robot physical interaction. *IEEE Robot Autom Lett* 3: 249–256, 2018. doi:10.1109/LRA.2017.2737048.
101. **Edraki M**, **Maurice P**, **Sternad D.** Humans need augmented feedback to physically track non-biological movements. *2023 IEEE International Conference on Robotics and Automation (ICRA)*. London, 2023.
102. **Miller DI**, **Nelson RC.** *Biomechanics of Sport: A Research Approach*. Philadelphia, PA: Lee and Febiger, 1973.
103. **Plagenhoef S.** *Patterns of Human Motion: A Cinematographic Analysis*. New York: Prentice-Hall, 1971.
104. **Al-Khazali HAH**, **Askari MR.** Geometrical and graphical representations analysis of lissajous figures in rotor dynamic system. *IOSRJEN* 2: 971–978, 2012. doi:10.9790/3021-0205971978.
105. **McIntyre J**, **Bizzi E.** Servo hypotheses for the biological control of movement. *J Mot Behav* 25: 193–202, 1993. doi:10.1080/00222895.1993.9942049.

Downloaded from journals.physiology.org/journal/jn at EPFL Bibliotheque USD (128.179.253.225) on January 16, 2024.